MRAS Speed Observer for High-Performance Linear Induction Motor Drives Based on Linear Neural Networks

Maurizio Cirrincione, *Senior Member, IEEE*, Angelo Accetta, *Member, IEEE*, Marcello Pucci, *Senior Member, IEEE*, and Gianpaolo Vitale, *Member, IEEE*

***Abstract*—This paper proposes a neural network (NN) model reference adaptive system (MRAS) speed observer suited for linear induction motor (LIM) drives. The voltage and current flux models of the LIM in the stationary reference frame, taking into consideration the end effects, have been first deduced. Then, the induced part equations have been discretized and rearranged so as to be represented by a linear NN (ADALINE). On this basis, the transport layer security EXIN neuron has been used to compute online, in recursive form, the machine linear speed. The proposed NN MRAS observer has been tested experimentally on suitably developed test set-up. Its performance has been further compared to the classic MRAS and the sliding-mode MRAS speed observers developed for the rotating machines.**

***Index Terms*—Field-oriented control (FOC), linear induction motor (LIM), model reference adaptive systems (MRASs), neural networks (NNs), sensorless control.**

NOMENCLATURE

$\mathbf{u}_s = u_{sD} + j\, u_{sQ}$	Space vector of the inductor voltages in the inductor reference frame.
$\mathbf{i}_s = i_{sD} + j\, i_{sQ}$	Space vector of the stator currents in the inductor reference frame.
$\boldsymbol{\psi}'_r = \boldsymbol{\psi}_{rd} + j\, \boldsymbol{\psi}_{rq}$	Space vector of the induced part flux-linkages in the stator reference frame.
ρ_r	Phase angle of the induced part flux linkage space vector with respect to the sD axis.
L_s	Inductor inductance.
L_r	Induced part inductance.
L_m	Three-phase magnetizing inductance.
$L_{\sigma s}$	Inductor leakage inductance.
$L_{\sigma r}$	Induced part leakage inductance.
R_s	Resistance of an inductor phase winding.
R_r	Resistance of the induced part.
p	Number of pole pairs.
ω_r	Angular induced part speed (in electrical angles per second).
v	Linear speed.
τ_m	Length of the inductor.
τ_p	Polar pitch.

I. INTRODUCTION

LITERATURE about linear induction motor (LIM) is huge [1]–[5]. The option that LIMs offer to develop a direct linear motion without the need of any gear box for the motion transformation (from rotating to linear) has been the key issue for their study. The counterpart of this potential advantage is the increase of complexity of the machine model, which presents the so-called end effects and border effects. These effects, which are due to asymmetries in the inductor structure with respect to the rotating machine, both in the longitudinal and in the transversal direction, make obtaining good control performance from the linear drive a difficult task. Speed control of the LIM, however, requires the adoption of a linear encoder, which is typically far more expensive and less reliable of the corresponding counterpart in the rotating machine. Moreover, in the LIM case, the cost of the encoder increases with the length of the induced part track, which could be very demanding in applications like railway traction systems and in general movement systems with long tracks. The possibility of adopting suited sensorless techniques [6], [7] is, thus, very interesting for these applications, where typically the linear encoder would also be exposed to potentially damaging environmental factors (sun, humidity, mechanical stress, etc.). In general, the problem of properly estimating the speed/position of an ac motor is still very challenging [8]–[11]. Very few applications of sensorless techniques suited for LIMs have been proposed in the literature, among which [12] and [13], probably because of the further increased complexity of a speed observer which should consider also the end effects of the machine. In particular, Huang *et al*. [12] propose a complex adaptive speed sensorless controller for the LIM, while Ryu *et al*. [13] propose a sensorless technique suited for LIMs based on high-frequency signal injection. This paper, which is an improvement of [14] and [15], proposes a neural network (NN) model reference adaptive

Manuscript received February 2, 2012; revised April 5, 2012; accepted May 7, 2012. Date of current version September 11, 2012. Recommended for publication by Associate Editor A. M. Trzynadlowski.

M. Cirrincione is with the Université Technologique de Belfort Montbeliard, 90010 Belfort, France (e-mail: m.cirrincione@ieee.org).

A. Accetta is with the Institute of Intelligent Systems for the Automation, Italian National Research Council, 90121 Palermo, Italy (e-mail: angelo.accetta@gmail.com).

M. Pucci and G. Vitale are with the Institute of Intelligent Systems for the Automation, Italian National Research Council, 90121 Palermo, Italy (e-mail: marcello.pucci@ieee.org; gianpaolo.vitale@ieee.org).

Color versions of one or more of the figures in this paper are available online at http://ieeexplore.ieee.org.

Digital Object Identifier 10.1109/TPEL.2012.2200506

system (MRAS) observer, where the adaptive model is a linear NN (ADALINE). In particular, it presents the experimental application of [14], where this method has been proposed only in numerical simulation. In [15], it has been shown in numerical simulation that the classic MRAS observer, modified only in the equations of its reference and adaptive models so as to include end effects, outperforms that based on the classic equations of the rotating induction machine (RIM) [16]. Moreover, in [15], it has been already demonstrated in numerical simulation that the NN MRAS observer including end effects improves the classic MRAS observer including end effects.

This application is the extension and upgrade of a set of MRAS observers, initially proposed for rotating machines [17], [18], suitably adapted to LIMs sensorless control. In particular, starting from the modified electrical circuit of the LIM [19], rearranged here in a space-vector fashion form, the voltage and current models of the LIM in the stationary reference frame, taking into consideration the end effects, have been deduced. Afterward, while the inductor equations have been directly used as reference model of the NN MRAS observer, the induced part equations have been discretized and rearranged so as to be represented by a linear NN (ADALINE). On this basis, the total least-squares (TLS) EXIN neuron has been used to compute on-line, in recursive form, the machine linear speed, since it reveals the best least-squares (LS) technique [20], [21] to solve online the linear problem under hand. The proposed NN MRAS observer has been tested experimentally on suitably developed test set-up. Its performance has been further compared to the classic MRAS speed observer and sliding mode (SM) MRAS observer for RIMs [16], [31].

II. Equivalent Circuit of the LIM Including End Effects

In a LIM, the secondary (induced part) consists of a sheet of aluminum with a back core of iron. During the motion of the inductor, the aluminum plate surface magnetically linked with the inductor varies in a continuous manner. This causes a variation of the induced currents in the sheet and corresponding magnetic flux density in the air gap, in proximity of the entrance (front of the motion) and exit (back of the motion) of the inductor. When the moving inductor faces a new part of aluminum sheet, new induced currents are generated starting from a null value. This growth, which is quite fast because of the absence of previously induced currents, tries to oppose to the inducing flux variation. The effect is a deep reduction of the resulting flux in proximity of the entrance. At the same time, at the exit, the induced current oppose to a sudden flux reduction from the inducer, creating an overall flux increase. The higher the speed of the inductor, the higher the end-effect phenomenon [22], [23]. This last has been taken into consideration in the literature by a so-called end-effect factor Q [19], defined as $Q = \tau_m R_r / (L_m + L_{\sigma r})\, v$, where τ_m is the length of the inductor, R_r and $L_{\sigma r}$ are the induced part resistance and leakage inductance, L_m is the three-phase magnetizing inductance, and v is the linear speed of the machine. It can be observed that the higher the machine speed, the higher the air-gap thickness (higher leakage inductance), the lower the inductor length, the lower the factor Q. It means that the end effects increase with the machine speed, with the air-gap thickness and reduces with the inductor length. Correspondingly, the three-phase magnetizing inductance varies with Q in the following way: $L'_m = L_m\ (1 - f\,(Q))$, with $f\,(Q) = 1 - e^{-Q}/Q$. A computation of the overall losses of the machine shows that a resistance appears in the transversal branch taking into consideration the eddy current joule losses. This resistance is equal to $R'_r = R_r\ f(Q)$. Correspondingly, the steady-state equivalent circuit [19] of the LIM is shown in Fig. 1, where it is sketched in a space-vector fashion form. It could be observed that the main differences with the equivalent circuit of the RIM are in the magnetizing inductance and in the eddy current resistance, both present in the transversal branch.

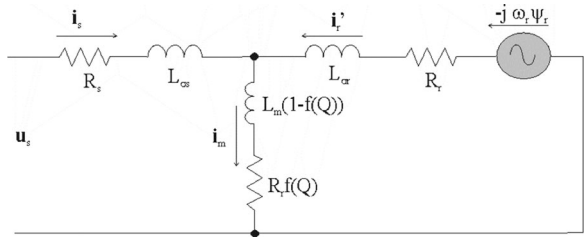

Fig. 1. Space-vector equivalent circuit of the LIM.

III. Field-Oriented Control (FOC) of the LIM

Several attempts to particularize FOC [24]–[26] and direct thrust control [27] to LIMs have been proposed in the literature. Here, a direct induced part flux-oriented control of the LIM has been adopted. The block diagram of the adopted control scheme is drawn in Fig. 2. In the adopted FOC scheme, current control is performed in the induced part flux-oriented reference frame. On the direct axis x, a flux control loop commands the direct current loop and a voltage control loop commands the flux loop to permit the drive to work automatically in the field weakening region by maintaining constant the product of the rotor flux amplitude and the absolute value of the inductor speed. On the quadrature axis y, a speed loop controls the quadrature current loop. It should be noted that the angular position ρ_r, needed for the correct field orientation, is provided by the NN MRAS observer and thus it implicitly takes into consideration the end effect of the LIM. All controllers used in the control loops are proportional integral type. An asynchronous space-vector pulsewidth modulation (SV-PWM) with $f_{\mathrm{PWM}} = 5\,\mathrm{kHz}$ has been used to command the inverter.

IV. Limits of Model-Based Sensorless Techniques

A. Open-Loop Integration

One of the main problems of many model-based speed observers, when adopted in high-performance drives, is the open-loop integration in presence of dc biases. Typically, MRAS observers based on flux error suffer from this problem. In particular, dc drifts are always present in the signal before it is integrated, which causes the integrator to saturate with a resulting inadmissible estimation error, and also after it is integrated

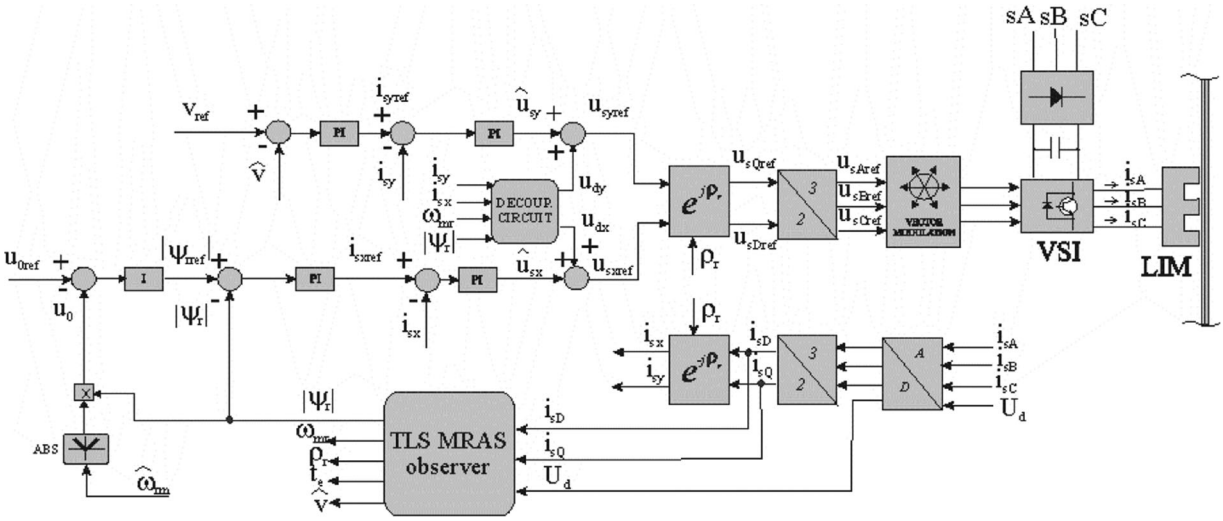

Fig. 2. Block diagram of the FOC of the LIM.

because of the initial conditions. In general, low-pass (LP) filters with very low cutoff frequency are used instead of pure integrators; however, since they fail to integrate in low-frequency ranges, close to their cutoff frequency, some alternative solutions can be used, e.g., the integrator with saturation feedback, the integrator based on cascaded LP filters, the integrator based on the offset vector estimation and compensation of residual estimation error, and the adaptive neural integrator [28]. In this case, the voltage model of the linear induction machine, used as a reference model of the NN MRAS observer, has been integrated with a neural integrator based on two linear adaptive filters [17], [18].

B. Inverter Nonlinearity

The inverter power devices present a finite voltage drop in "on-state," due to their forward nonlinear characteristics. This voltage drop has to be taken into consideration at low frequency (low-voltage amplitude), where it becomes comparable with the stator voltage itself, giving rise to distortion and discontinuities in the voltage waveform. The proposed MRAS NN observer adopts the compensation method in [29] which is based on modeling the forward characteristics of each power device by using a piecewise linear characteristics, with an average threshold voltage and with an average differential resistance.

C. Machine Parameter Mismatch

A further source of error in flux estimation is the mismatch of the stator (inductor in the LIM) and rotor (induced part in the LIM) resistances of the observer with their real values because of heating/cooling of the machine, e.g., the load-dependent variations of the winding temperature may lead up to 50% error in the modeled resistance. Stator and rotor resistances should be, therefore, estimated online and tracked during the operation of the drive. In any case, it should be remarked that the steady-state estimation of the rotor resistance cannot be performed in sensorless drives; thus, rotor resistance variations must be deduced from the stator resistance estimation. In this case, the voltage model of the induction machine, used as a reference model of the NN MRAS observer, integrated with the stator resistance estimation algorithm proposed in [30] has been used. It is based on the minimization of the error between the measured $i_{sx}^{\psi_s}$ and estimated $\hat{i}_{sx}^{\psi_s}$ direct component of the stator current space vector in the stator flux reference frame (apex indicates the reference frame in which space vectors are expressed).

V. NN MRAS Observer

Following the logic of MRAS observer [16], the estimated speed is obtained on the basis of the induced part flux linkage error. The proposed NN MRAS speed observer, taking into consideration the end effects of the LIM, is based on the inductor and induced part space-vector equations written in the inductor reference frame.

On the basis of the circuital representation drawn in Fig. 1, after some algebraic manipulations, the following space-vector equations, valid, respectively, for the inductor and the induced part, can be obtained in the inductor reference frame:

$$\frac{d\boldsymbol{\psi}'_r}{dt} = \mathbf{u}_s - R_s\,\mathbf{i}_s - L_{\sigma s}\,\frac{d\,\mathbf{i}_s}{dt} - \frac{R_r\,f\,(Q)}{L_m\,(1-f\,(Q))}\boldsymbol{\psi}'_r \quad (1)$$

$$\frac{d\boldsymbol{\psi}'_r}{dt} = R_r\,\mathbf{i}_s + \left(j\frac{p\pi}{\tau_p}\,v - \frac{R_r\,(1+f\,(Q))}{L_m\,(1-f\,(Q))}\right)\boldsymbol{\psi}'_r \quad (2)$$

For the symbols, see the Nomenclature.

Equations (1) and (2) have been computed under the simplifying assumption that the leakage factor of the induced part is null and the rate of change of the linear speed is almost null, i.e., $(dv/dt) \cong 0$; otherwise, some additive terms depending on the linear acceleration of the motor would appear. Equation (1) represents the so-called voltage model, which is based on the inductor equations, while (2) represents the so-called current model, which is based on the induced part equations. It should be noted that the voltage model presents, with respect to the RIM model, an additive term, depending on the induced part flux linkage and on the end factor Q; this term would be zero if no end effect existed. It should be further noted that the current

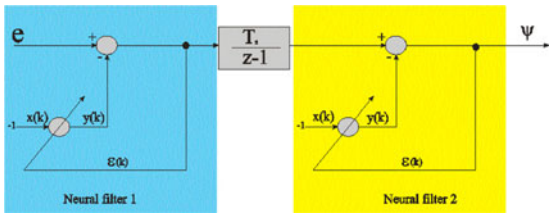

Fig. 3. Neural adaptive integrator.

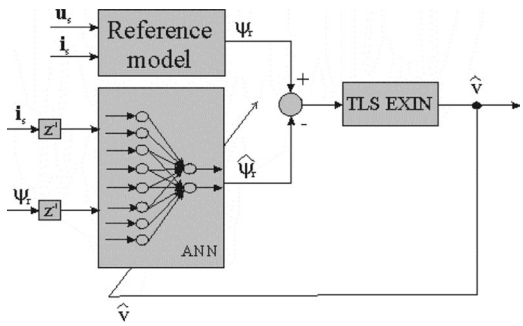

Fig. 4. Block diagram of the NN MRAS speed observer.

model is written as a function of the linear speed of the motor, instead of the electrical rotating speed, being the relationship between the two the following: $\omega_r = (p\pi/\tau_p)v$. It is basically the same equation of the RIM, where an equivalent induced part time constant depending on the end effects is to be defined as $\tau_t' = L_m\ (1 - f\,(Q))\,/R_r\,(1 + f\,(Q))$. Following the logic of the NN MRAS observers for RIMs in [17] and [18], (1) has been used as a reference model since its dependence on the speed, due only to the additive term, can be neglected at the first instance. It should be noted, in any case, that the variability of the reference model with the linear speed is limited because it influences only the time constant with which the flux converges to its final value and to its phase angle.

A. Neural Adaptive Integrator

To solve the dc drift and initial condition problems caused by the open-loop integration of the flux, the so-called neural adaptive integrator has been adopted [17], [18], [28]. The idea is to use a linear filter (ADALINE) used as a notch filter to cutoff the dc component adaptively.

The learning law of the neural adaptive filter is as follows:

$$y\,(k+1) = y\,(k) + 2\tau\,(d\,(k) - y\,(k)) \tag{3}$$

where k is the current time instant, $d(k)$ is the primary input of the filter, $y(k)$ is the output of the filter neuron, and τ is the learning rate. This one-weight neuron is able to remove not only a constant bias but also a slowly varying drift in the primary input. It should be remarked that two neural filters must be used in the neural-based integrator: the neural filter 1 eliminates the dc component of the signal to be processed, and the neural filter 2 eliminates the dc drift appearing at the output of the integrator because of the initial conditions and the filtering error of the neural filter 1 appearing during its adaptation (see Fig. 3). In this case, to improve the accuracy of the induced part flux estimation, the neural adaptive filter has been further improved by making its learning rate τ variable with the machine speed, as fully described in [18].

B. NN Adaptive Model

Equation (2) has been used to derive the neural adaptive model, because of its explicit dependence on the speed. The adaptive model is here an ADALINE (linear neural network), which reproduces the induced part equations (2) of the LIM (current model). The speed is then computed by employing the induced part flux linkage error between the voltage and the current models. The block diagram of the neural MRAS speed observer is sketched in Fig. 4. After projecting the vector equation (2) in the real and quadrature axis, and converting both equations from the continuous to the discrete time domain by the Euler method, the following equations can be retrieved:

$$\begin{cases} \boldsymbol{\psi}'_{rd}\,(k) = \boldsymbol{\psi}'_{rd}\,(k-1) + R_r\,T_s\,i_{sD}\,(k-1) \\ \qquad -\frac{p_p\,\pi\,T_s}{\tau_m}\,v\,(k-1)\,\boldsymbol{\psi}'_{rq}\,(k-1) \\ \qquad -\frac{R_r\,T_s\,(1+f(Q))}{L_m\,(1-f(Q))}\,\boldsymbol{\psi}'_{rd}\,(k-1) \\ \boldsymbol{\psi}'_{rq}\,(k) = \boldsymbol{\psi}'_{rq}\,(k-1) + R_r\,T_s\,i_{sQ}\,(k-1) \\ \qquad +\frac{p_p\,\pi\,T_s}{\tau_m}\,v\,(k-1)\,\boldsymbol{\psi}'_{rd}\,(k-1) \\ \qquad -\frac{R_r\,T_s\,(1+f(Q))}{L_m\,(1-f(Q))}\,\boldsymbol{\psi}'_{rq}\,(k-1) \end{cases} \tag{4}$$

where k is the current time sample and T_s is the sampling time of the control system. Equation (4) can be rewritten in this way

$$\begin{cases} \hat{\psi}'_{rd}\,(k) = w_1\,\hat{\psi}'_{rd}\,(k-1) - w_2\,\hat{\psi}'_{rq}\,(k-1) + w_3\,i_{sD}\,(k-1) \\ \hat{\psi}'_{rq}\,(k) = w_1\,\hat{\psi}'_{rq}\,(k-1) + w_2\,\hat{\psi}'_{rd}\,(k-1) + w_3\,i_{sQ}\,(k-1). \end{cases} \tag{5}$$

The $\hat{}$ symbol has been used to connote the flux estimated with the current model. Equation (5) can be looked at as the equation of a linear NN (ADALINE) with four inputs and two outputs, whose weights are defined as follows:

$$w_1 = 1 - \frac{R_r\,T_s\,(1+f\,(Q))}{L_m\,(1-f\,(Q))}$$
$$w_2 = \frac{p\pi\,T_s}{\tau_p}\,v\,(k-1)\,, \quad w_3 = R_r\,T_s \tag{6}$$

It should be remarked that the values of the induced part flux-linkage components at the input of the artificial NN (ANN) are those coming from the reference model, and not from the adaptive one. The NN is, therefore, not used in the usual "*simulation*" mode, where its delayed output is used as its input, but in the "*prediction*" mode, the delayed output of the voltage model is used as input to the NN, which allows a quicker and more stable convergence of the estimation algorithm.

As for the weights, w_3 is a constant, w_1 presents an indirect dependence on the machine speed on the basis of the $f(Q)$ function, while w_2 presents a direct dependence on the machine speed. From this standpoint, (5) can be written in the following matrix form, considering the fact that the ANN is used as a

predictor and not as a simulator:

$$\begin{bmatrix} \psi'_{rq}(k-1) \\ -\psi'_{rd}(k-1) \end{bmatrix} w_2 = \begin{bmatrix} \hat{\psi}'_{rd}(k) - w_1\,\psi'_{rd}(k-1) - w_3\,i_{sD}(k-1) \\ \hat{\psi}'_{rq}(k) - w_1\,\psi'_{rq}(k-1) - w_3\,i_{sQ}(k-1) \end{bmatrix}. \quad (7)$$

In the ANN, the weight w_3 is kept constant to its values computed offline, while w_2 is adapted online by means of the TLS EXIN algorithm. As far as w_1 is concerned, its dependence on the machine speed due to the *f(Q)* function is included as a modeling error to be covered by the LS algorithm. The w_1 weight is, however, updated at each sampling time, on the basis of the previous sampled value of the estimated speed; it means that the *f(Q)* is updated with a single sampling time delay with respect to the current estimated speed.

C. TLS EXIN Speed Estimation

The linear matrix equation (7), which can be written more generally as $\mathbf{Ax} \approx \mathbf{b}$, can be solved for v by using LS techniques. In particular in the literature, there exist three LS techniques, i.e., the ordinary LS (OLS), the total LS (TLS), and the data LS (DLS) which arise when errors are, respectively, present only in **b** or in both **A** and **b** or only in **A**.

In classical OLS, each element of **A** is considered without any error; therefore, all errors are confined to **b**. However, this hypothesis does not always correspond to the reality: modeling errors, measurement errors, etc., can in fact cause errors also in **A**. Therefore, in real-world applications, the employment of TLS would be very often better, as it takes into consideration also the errors in the data matrix. This is certainly the case of speed estimation, where the estimated induced part flux, present in **A**, is affected both by modeling errors and noise. Therefore, a TLS technique should be used instead of the OLS technique. The TLS EXIN neuron has been adopted here, which is the only NN capable to solve a TLS problems recursively online. For details on the TLS EXIN Neuron theory, refer to [20] and [21]. The final recursive adaptation law for the estimated linear speed is the following, retrieved on the basis of a gradient descent rule

$$\hat{v}(k+1) = \hat{v}(k) - \alpha(k)\ \boldsymbol{\gamma}(k)\ \mathbf{a}^T(k) + \left[\alpha(k)\ \boldsymbol{\gamma}^2(k)\right]\hat{v}(k) \quad (8)$$

where k is the current time sample, $\mathbf{a}(k)$ is the kth 2-element column vector of **A**, α is a positive constant, and $\boldsymbol{\delta}(k)$ and $\boldsymbol{\gamma}(k)$ are defined as

$$\begin{cases} \gamma(k) = \dfrac{\delta(k)}{1+\hat{v}^2} \\ \delta(k) = \dfrac{(\mathbf{a}(k)\ \hat{v} - \mathbf{b}(k))}{1+\hat{v}^2} \end{cases} \quad (9)$$

where **b**(k) is the corresponding two-element observation vector.

VI. Test Set-up

A test set-up has been suitably built to test the NN MRAS speed observer taking into consideration the LIM end effects. The machine under test is a LIM model Baldor LMAC1607C23D99, whose rated data and electrical parameters are shown in Table I. The LIM has been equipped with a linear encoder Numerik Jena LIA series, used only to verify the goodness of the NN MRAS speed estimation. The estimated speed has been fed back to the speed controller to close the speed loop. The LIM presents an induced part track of length 1.6 m.

TABLE I
Parameters of the LIM

Rated power P_{rated} [W]	424.7
Rated voltage U_{rated} [V]	380
Rated frequency f_{rated} [Hz]	60
Pole-pairs	3
Inductor resistance R_s [Ω]	11
Inductor inductance L_s [mH]	637.6
Induced part resistance R_r [Ω]	32.57
Induced part inductance L_r [mH]	757.8
3-phase magnetizing inductance L_m [mH]	517.5
Rated thrust F_n [N]	200
Rated speed [m/s]	6.85
Mass [kg]	20

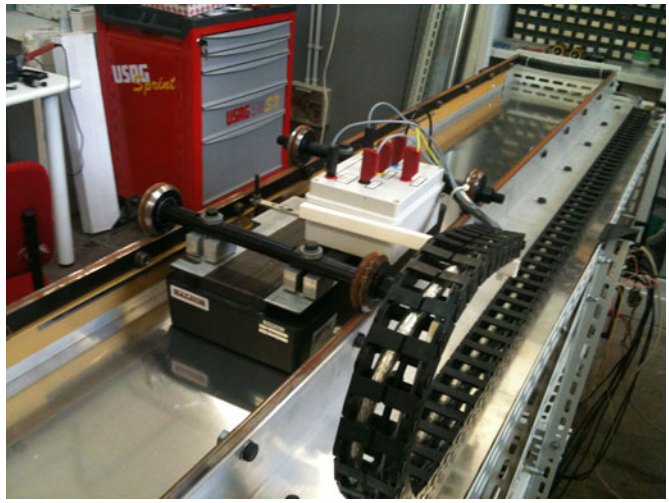

Fig. 5. Experimental test set-up.

The employed test set-up consists of:

1) a three-phase LIM with parameters shown in Table I;
2) a frequency converter which consists of a three-phase diode rectifier and a 7.5 kVA, three-phase voltage source inverter;
3) a dSPACE card (DS1103) with a PowerPC 604e at 400 MHz and a floating-point DSP TMS320F240.

Fig. 5 shows a photograph of the test set-up.

VII. Experimental Results

The NN MRAS speed observer taking into consideration the LIM end effects has been tested experimentally on the test set-up described in Section VI. Its performance has been verified in several challenging working conditions. All the following tests have been done with the estimated speed fed back to the speed control loop, differently from those done with the other observers in the following. The first test consists of square speed references at low speed, with steps, respectively, from 0.8

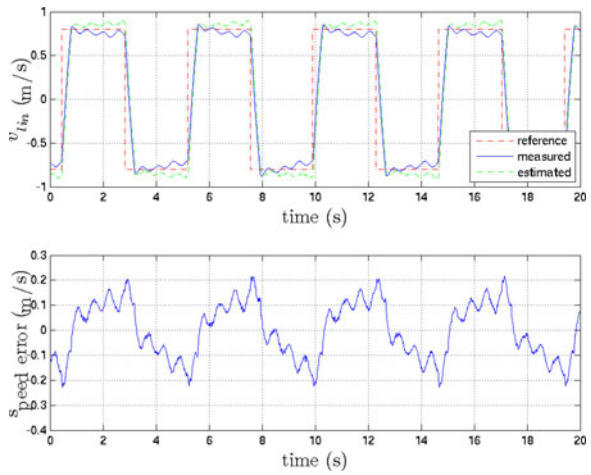

Fig. 6. Reference, estimated, and measured speed during reversals from 0.8 to −0.8 m/s with the NN MRAS.

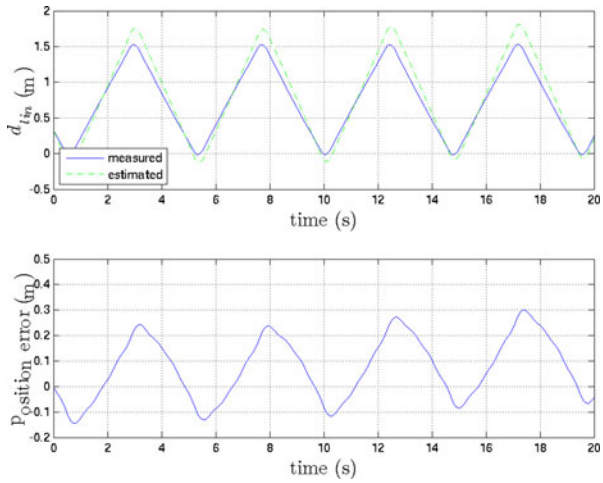

Fig. 7. Estimated and measured position during reversals from 0.8 to −0.8 m/s with the NN MRAS.

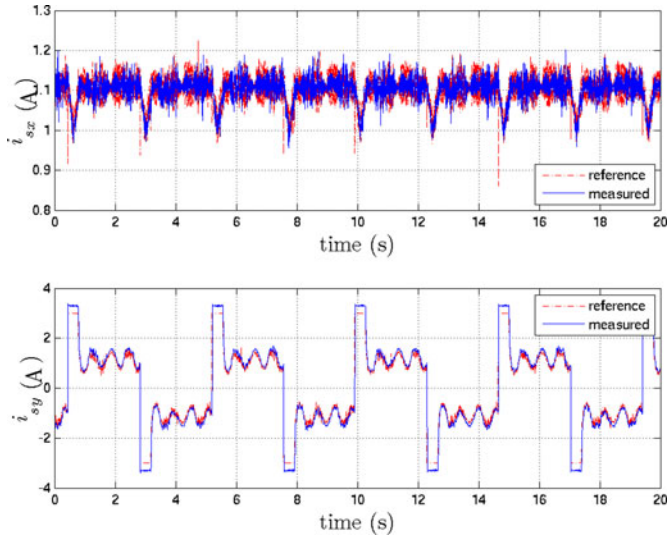

Fig. 8. Reference and measured i_{sx} and i_{sy} current components during reversals from 0.8 to −0.8 m/s with the NN MRAS.

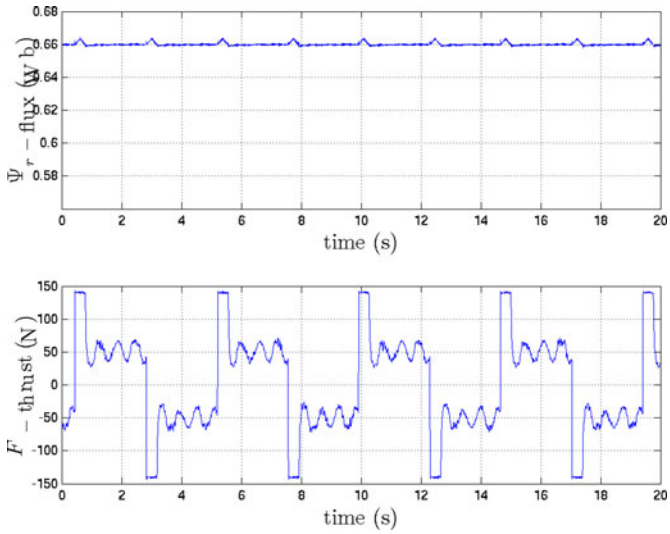

Fig. 9. Induced part flux ψ_r and thrust F during reversals from 0.8 to −0.8 m/s with the NN MRAS.

to −0.8 m/s and from 0.2 to −0.2 m/s (corresponding, respectively, to about 11% and 3% of the rated speed). The frequency of the square speed reference is determined by the length of the track (1.6 m): whenever the inductor reaches the end of the track, the sign of the speed reference is changed. The higher the peak speed, the higher the frequency of the square reference. Fig. 6 (11) shows the reference, the estimated, and the measured speed, as well as the instantaneous speed estimation error during the 0.8 → −0.8 m/s (0.2 → −0.2 m/s) test. Fig. 7 (Fig. 12) shows the corresponding estimated and measured position, Fig. 8 (Fig. 13) shows the i_{sx} and i_{sy} current components, which are the direct quadrature components of the inductor currents in the induced part flux reference frame, and finally Fig. 9 (Fig. 14) shows the induced part flux amplitude and the thrust of the LIM. It should be noted that, in both tests, the estimated speed properly tracks its reference and the measured one, as expected (the estimated speed is fed back to the control system, while the measured speed is used only for comparison). The percent average absolute speed estimation error is almost equal to 11% for the 0.8 → −0.8 m/s test and to 22% for the 0.2 → −0.2 m/s test. As expected, the lower the reference speed, the higher the average absolute speed estimation error. Correspondingly, the average absolute position estimation error is almost equal to 0.07 m for the 0.8 → −0.8 m/s test and to 0.09 m for the 0.2 → −0.2 m/s test, which is very low in both cases. In this regard, it should be noted that not only the speed reference is very low in both tests, but also the LIM drive is as a matter of fact loaded (almost 30% of the rated load, as it can be observed from the thrust curves), just because of the friction force of the system due to the inductor insisting on the guides. The inductor current curves highlight a proper field orientation, with i_{sx} correctly controlled to a constant value and i_{sy} suddenly varying at each speed reversal and controlled to a constant non-null value at speed steady state (due to the friction load). Moreover, the response of the current control loop to sudden variation is fast. The induced part flux and the thrust curves present the

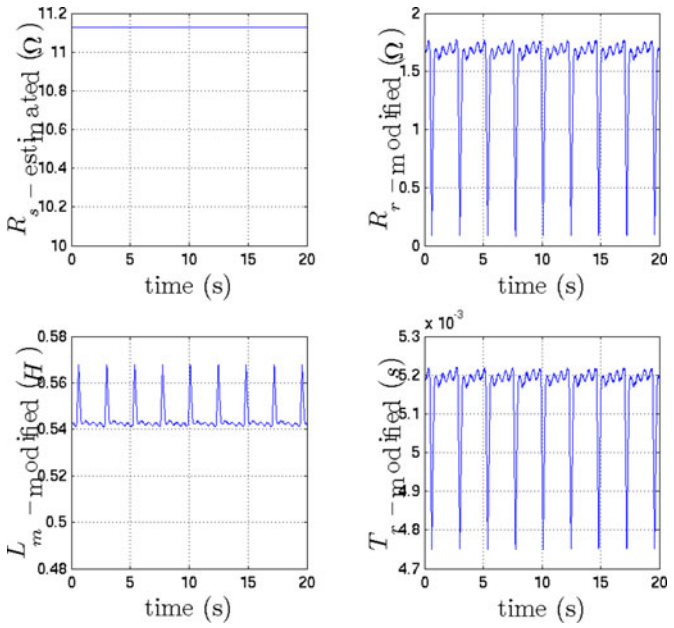

Fig. 10. Estimated parameters of the LIM during reversals from 0.8 to −0.8 m/s with the NN MRAS.

same shape of the current ones, as expected. Finally, Fig. 10 shows the stator resistance estimated online with the algorithm [30] and the modified parameters of the LIM electrical circuit model in Fig. 1—$R'_r = R_r\, f(Q)$, $L'_m = L_m\,(1 - f(Q))$, and $\tau'_r = L_m\,(1 - f(Q))/R_r\,(1 + f(Q))$—taking into consideration the end effects, as computed by the NN MRAS observer during the $0.8 \rightarrow -0.8$ m/s test. It can be observed that the inductor resistance is correctly estimated online, which makes the reference model properly tuned even at low operating speed; moreover, the modified induced part resistance and time constant increase with the linear speed, while the magnetizing inductance reduces with it, as expected. The important feature for which the NN MRAS observer accounts for the variations of the parameters of the LIM with speed explains the correct behavior of the LIM drive during the speed reversals. When the linear speed changes its sign passing for zero, the modified induced part time constant reduces significantly and correspondingly, if this effect is not properly considered, the correct field orientation can be lost, as will be shown in Sections VII-A and VII-B for the cases of the classic MRAS and the sliding-mode (SM) MRAS observers, respectively. Finally, the current figures exhibit, particularly that obtained at 0.8 m/s, a low-frequency ripple on both i_{sy} and i_{sy}, resulting in a corresponding ripple on the thrust and finally on the speed. This ripple evidences the presence of a nonperfect decoupling of the direct and quadrature current components, which could be explained because of the nonuniform air gap of the machine (the distance between the inductor and the aluminum track is not perfectly constant—some sinkings, for example, are present on the track) introducing space harmonics of the machine inductance. This is cause of a ripple of the thrust reflecting in a ripple of the speed, as observable. The possible reduction of such effect is out of the scope of this paper and will be addressed in future.

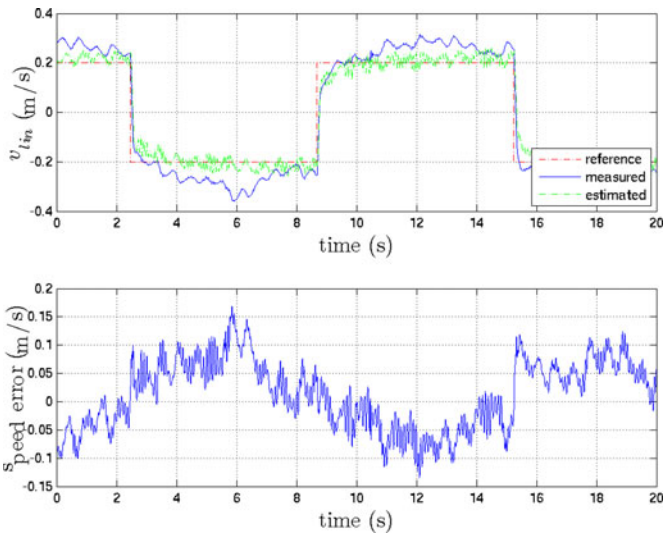

Fig. 11. Reference, estimated, and measured speed during reversals from 0.2 to −0.2 m/s with the NN MRAS.

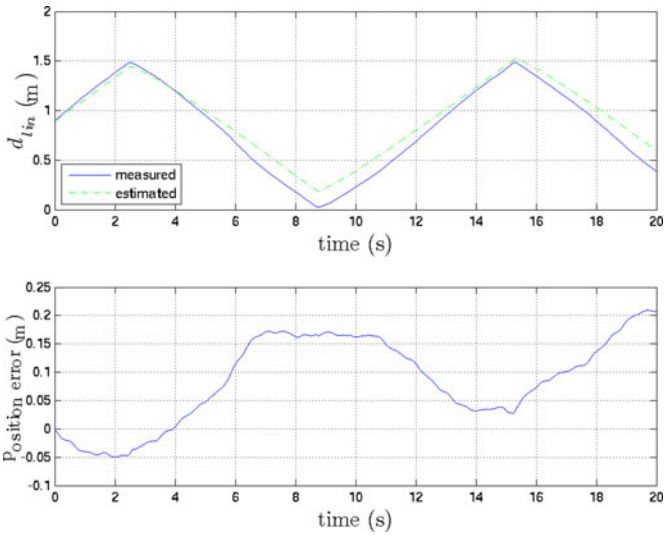

Fig. 12. Estimated and measured position during reversals from 0.2 to −0.2 m/s with the NN MRAS.

The second test consists of a startup of the drive at low speed, $0 \rightarrow 0.4$ m/s, with the LIM fully magnetized at zero speed, followed by a speed reversal $0.4 \rightarrow -0.4$ m/s. Figs. 15–18 show the same kind of waveforms shown in the former tests. Even in this test, the estimated speed is fed back to the speed control loop. Figures show that the LIM sensorless drive is able to properly work at zero speed at no load, with the machine fully magnetized. Moreover, the dynamic performance of the drive during the speed startup at low speed is good, with an instantaneous peak speed estimation error of 0.1 m/s. This is confirmed also by the i_{sx} and i_{sy} current components and thrusts/flux curves.

In the end, to fully characterize the behavior of the proposed NN MRAS observer, a high-speed reversal test has been performed. This test has been done only in numerical simulation since, as recalled previously, the induced part track has a limited length of 1.6 m, and therefore, the inductor cannot practically

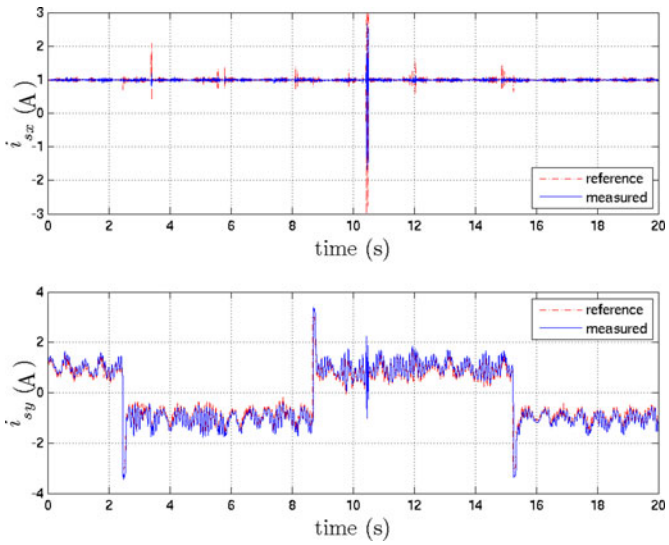

Fig. 13. Reference and measured i_{sx} and i_{sy} current components during reversals from 0.4 to -0.4 m/s with the NN MRAS.

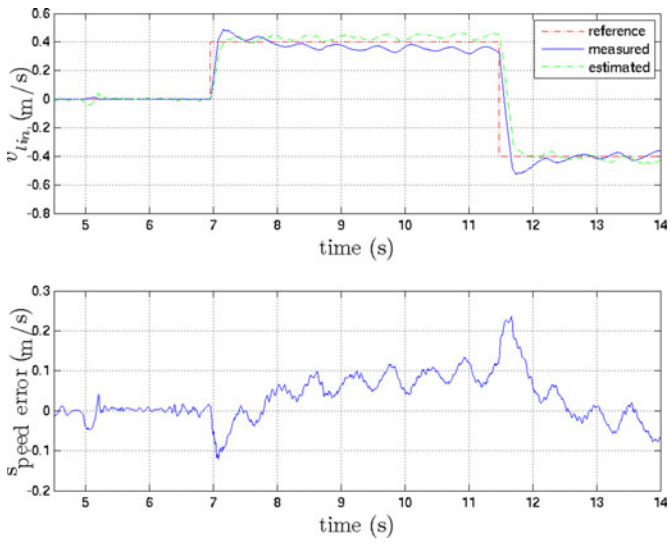

Fig. 15. Reference, estimated, and measured speed during a startup 0–0.4 m/s with the NN MRAS.

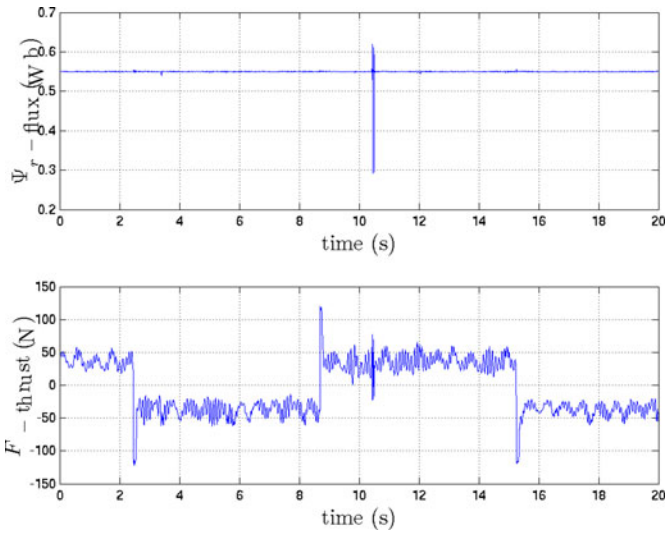

Fig. 14. Induced part flux ψ_r and thrust F during reversals from 0.4 to -0.4 m/s with the NN MRAS.

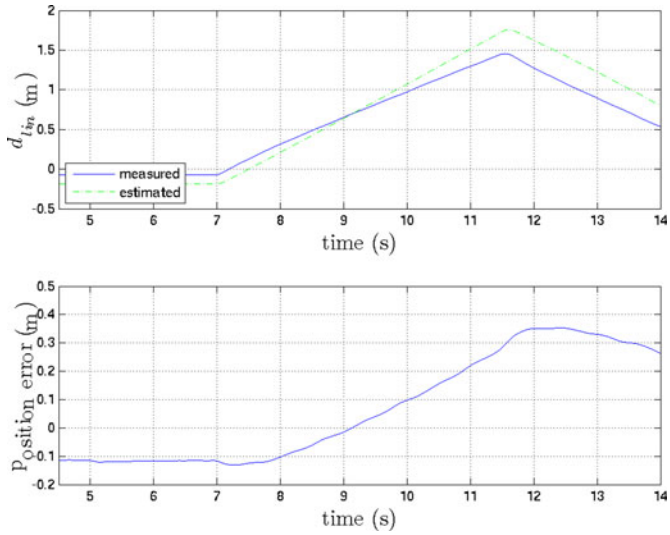

Fig. 16. Estimated and measured position during a start-up 0–0.4 m/s with the NN MRAS.

reach speeds above 1 m/s. To suitably check the proposed flux models taking into consideration the LIM end effects, as "machine under test" used in the simulations, the dynamic model of the LIM proposed in [32] and [33] has been implemented. This last model is based on the structural characteristics of the LIM (length of the inductor, number of slots, thickness of the induced part track, etc.) differently from the MRAS observer, which is based on the electrical parameters of the machine. In this way, the "machine under test" does not implement the same equations of the observer; consequently, the real capability of the MRAS observer to accurately estimate the machine speed and flux can be properly tested. Finally, it should be noted that the most problematic issues of sensorless control do not have significant effect at high speed. The simulation should, thus, provide a realistic picture of the real LIM drive behavior. The drive has been given a speed step from 0 to 6.8 m/s (rated speed), then a speed reversal from 6.8 to -6.8 m/s. Fig. 19 shows, respectively, the reference, measured, and estimated speed as well as the speed estimation error. Fig. 20 shows the direct and quadrature current components i_{sx} and i_{sy} during such a test. It could be noted that the drive is able to fully accomplish the speed reversal with the estimated speed properly tracking the measured one, and a speed estimation error never exceeding 1 m/s, even during transients. The current curves show a proper field orientation behavior with a constant direct current component and a square type quadrature component, each step occurring during the speed variation commands.

To verify the improvements achievable with the proposed NN MRAS observer taking into consideration the LIM end effects, some experimental comparisons with other MRAS techniques in the literature have been made. The adopted test set-up is that described in Section VI. In particular, the proposed observer

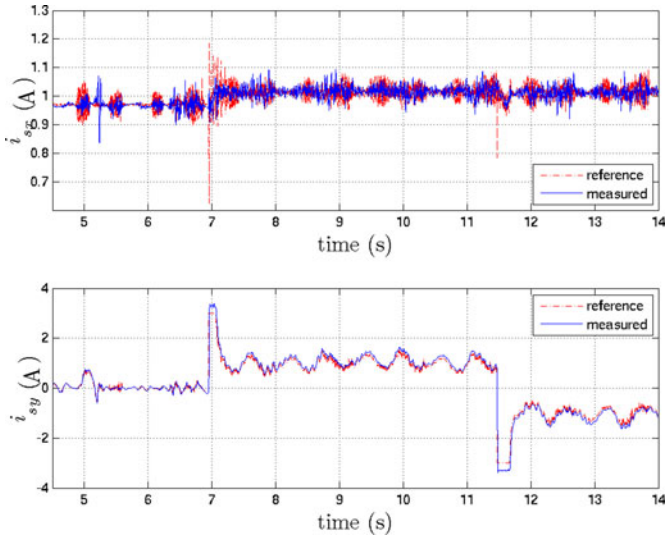

Fig. 17. Reference and measured i_{sx} and i_{sy} current components during a startup 0–0.4 m/s with the NN MRAS.

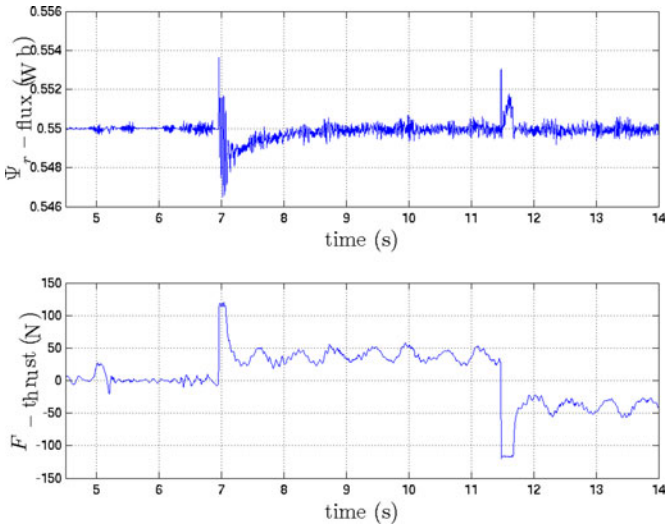

Fig. 18. Induced part flux ψ_r and thrust F during a startup 0–0.4 m/s with the NN MRAS.

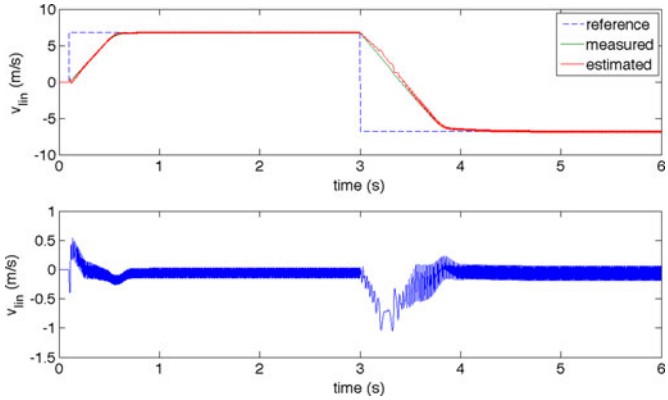

Fig. 19. Reference, estimated, and measured speed during the speed reversal from 6.8 to −6.8 m/s with the NN MRAS.

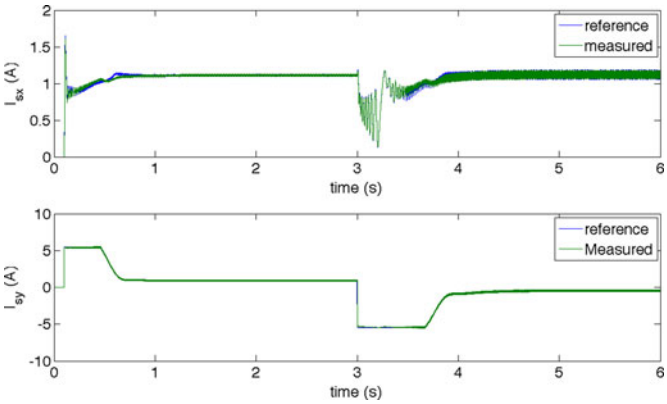

Fig. 20. Reference and measured i_{sx} and i_{sy} current components during the speed reversal from 6.8 to −6.8 m/s with the NN MRAS.

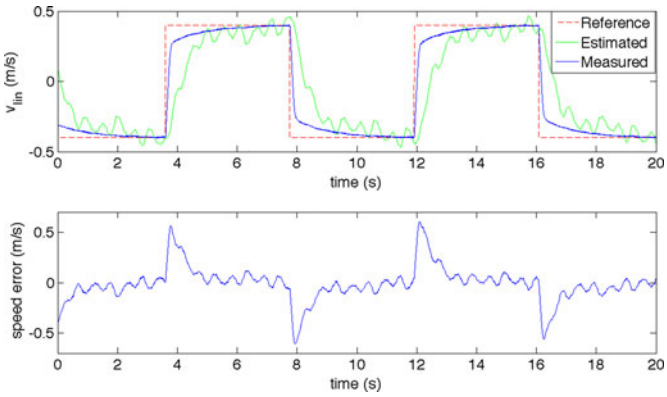

Fig. 21. Reference, estimated, and measured speed during reversals from 0.4 to −0.4 m/s with the classic MRAS.

has been compared with two analogous MRAS observers based on the flux error minimization: the classic MRAS observer [16] and the SM MRAS [31]. Both these two techniques have been originally devised for the RIM and just rearranged here to be adopted straightforwardly for the LIM.

A. Comparison With the Classic MRAS

The classic MRAS observer has been tuned on the basis of a tradeoff between the requirements of high dynamic performance and the limitation of the ripple of the estimated speed at steady state. It has been experienced that the classic MRAS observer, whatever is its tuning, needs a LP filtering of the estimated speed. It has been further experienced that the straightforward application of the classic MRAS devised for RIM to the LIM does not permit the speed loop to be closed on the estimated speed. In such an operation, the drive's behavior becomes unstable; these considerations confirm the improvements achievable thanks to both the proper modeling of LIM, taking into consideration the end effects, and the TLS EXIN training of the NN adaptive model. The following tests refer, thus, to an operation of the LIM drive where the speed signal fed back to the speed control loop is the measured one. Figs. 21 and 22 show the same kind of speed waveforms, as shown for the NN MRAS observer, obtained with the classic MRAS observer during two square speed reference tests, respectively, from 0.4 to −0.4 m/s and from

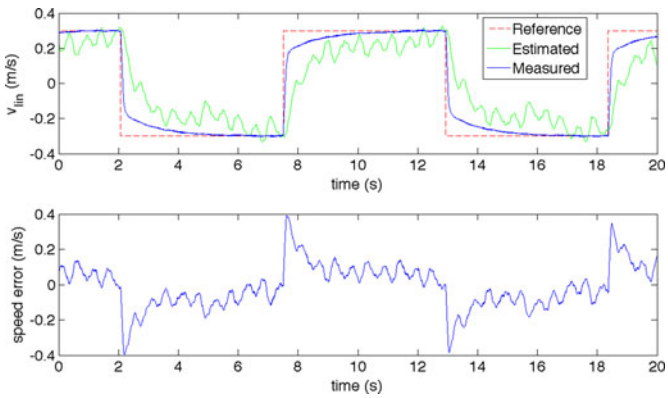

Fig. 22. Reference, estimated, and measured speed during reversals from 0.3 to −0.3 m/s with the classic MRAS.

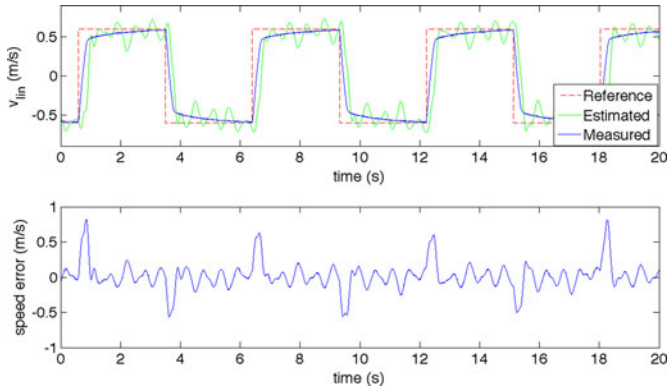

Fig. 23. Reference, estimated, and measured speed during reversals from 0.6 to −0.6 m/s with the SM MRAS.

0.3 to −0.3 m/s. These curves show that while at 0.4 m/s, the steady-state accuracy of the speed estimation is good, at 0.3 m/s, it decreases significantly with a speed estimation error around 0.1 m/s (33% of the reference). In both cases, the ripple of the estimated speed (after LP filtering) is significant and the speed estimation error during the transient is very high (more than 100% of the reference value). As a matter of fact, the estimated speed tracks the measured one with large delays. Increasing the proportional and integral gain of the MRAS observer would not be feasible, since it would cause a further increase of the ripple at steady state.

B. Comparison With the SM MRAS

One interesting variant and evolution of the classic MRAS observer is its SM version. The SM-MRAS observer has been proposed by Comanescu and Xu [31] in two different variants, called, respectively, single-manifold SM observer and double-manifold SM observer. In the following, some tests performed with the single-manifold SM MRAS observer are presented (see [31, scheme Fig. 7]). Even the SM MRAS observer is based on the flux error minimization, as the classic one, and is based on the classic model of the RIM, which is here rearranged to be used for the LIM. It has been experienced, even in this case, that the straightforward application of the classic MRAS devised for RIM to the LIM does not permit the speed loop to be closed on the estimated speed. In such an operation, the drive's behavior becomes unstable; these considerations further confirm the improvements achievable thanks to both the proper modeling of LIM, taking into consideration the end effects, and the TLS EXIN training of the NN adaptive model. Even in this case, the gain M of the observer has been chosen on the basis of a tradeoff between the stability issue and the dynamic performance issue. Figs. 23–25 show the same kind of speed waveforms, as shown for the NN MRAS observer, obtained with the SM MRAS observer during three square speed reference tests, respectively, from 0.6 to −0.6 m/s, from 0.4 to −0.4 m/s, and from 0.3 to −0.3 m/s. These curves show that while at 0.6 and 0.4 m/s, the steady-state accuracy of the speed estimation is good, at 0.3 m/s, it decreases significantly with a speed estimation error around 0.1 m/s (33% of the reference as in the classic MRAS). As far as the ripple at steady state (after LP filtering) is concerned, it is acceptable at 0.6 m/s, becoming very high at 0.3 m/s. As far as the transient behavior is concerned, a significantly faster response than the classic MRAS observer can be observed.

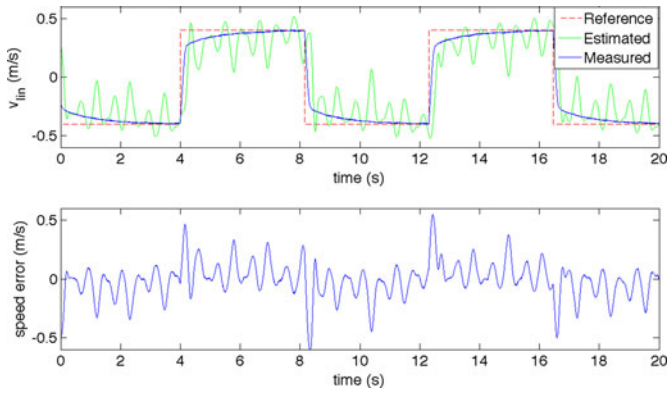

Fig. 24. Reference, estimated, and measured speed during reversals from 0.4 to −0.4 m/s with the SM MRAS.

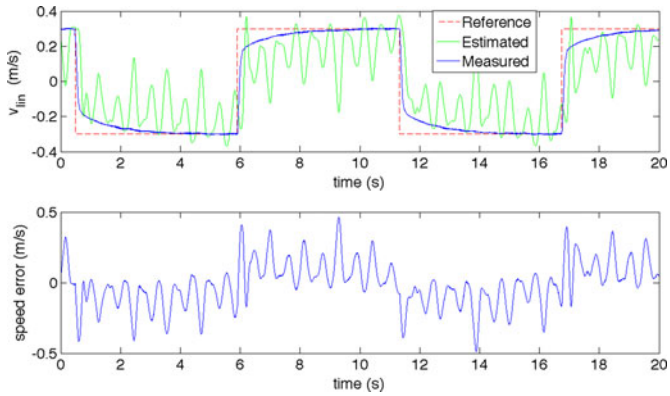

Fig. 25. Reference, estimated, and measured speed during reversals from 0.3 to −0.3 m/s with the SM MRAS.

VIII. Conclusion

This paper proposes an NN MRAS speed observer suited for LIM drives. Starting from the modified equivalent circuit of the LIM, the voltage and current models of the LIM in the stationary

reference frame, taking into consideration the end effects, have been deduced. Afterward, while the inductor equations have been used as a reference model of the NN MRAS observer, the induced part equations have been discretized and rearranged so as to be represented by a linear NN (ADALINE). On this basis, the so-called TLS EXIN neuron has been used to compute online, in recursive form, the machine linear speed. The proposed NN MRAS observer has been experimentally implemented on a suitably developed test set-up. Results show the performance of the proposed observer, working properly even at low speed in presence of load forces with good dynamic performance. Its performance has been further compared to the classic MRAS and sliding mode MRAS speed observers for RIMs.

REFERENCES

[1] E. R. Laithwaite, "Linear electric machines—A personal view," *Proc. IEEE*, vol. 63, no. 2, pp. 250–290, Feb. 1975.

[2] S. Yamamura, *Theory of the Linear Induction Motor*. New York: Wiley, 1972.

[3] I. Boldea and S. Nasar, *Linear Electric Motors*. Englewood Cliffs, NJ: Prentice-Hall, 1987.

[4] I. Boldea and S. Nasar, *Linear Motion Electromagnetic Devices*. New York: Taylor & Francis, 2001.

[5] I. Boldea and S. A. Nasar, *Linear Electric Actuators and Generators*. Cambridge, U.K.: Cambridge Univ. Press, 1997.

[6] K. Rajashekara, A. Kawamura, and K. Matsuse, *Sensorless Control of AC Motor Drives*. New York: IEEE Press, 1996.

[7] J. Holtz, "Sensorless control of induction motor drives," *Proc. IEEE*, vol. 90, no. 8, pp. 1359–1394, Aug. 2002.

[8] Y. Zhang, J. Zhu, Z. Zhao, W. Xu, and D. G. Dorrell, "An improved direct torque control for three-level inverter-fed induction motor sensorless drive," *IEEE Trans. Power Electron.*, vol. 27, no. 3, pp. 1502–1513, Mar. 2012.

[9] L. de Henriques, L. Rolim, W. Suemitsu, J. A. Dente, and P. J. Branco, "Development and experimental tests of a simple neurofuzzy learning sensorless approach for switched reluctance motors," *IEEE Trans. Power Electron.*, vol. 26, no. 11, pp. 3330–3344, Nov. 2011.

[10] S. Pongam and S. Sangwongwanich, "Stability and dynamic performance improvement of adaptive full- order observers for sensorless PMSM drive," *IEEE Trans. Power Electron.*, vol. 27, no. 2, pp. 588–600, Feb. 2012.

[11] J. S. Park, S. M. Jung, H. W. Kim, and M. J. Youn, "Design and analysis of position tracking observer based on instantaneous power for sensorless drive of permanent magnet synchronous motor," *IEEE Trans. Power Electron.*, vol. 27, no. 5, pp. 2585–2594, May 2012.

[12] C.-I. Huang, F. Li-Chen, W.-Y. Jywe, and J. C. Shen, "Speed motion-sensorless with adaptive control approach of linear induction motor unknown resistance and payload," in *IEEE Power Electron. Spec. Conf.*, Jun. 15–19, 2008, pp. 3887–3893.

[13] H.-M. Ryu, J.-I. Ha, and S.-K. Sul, "A new sensorless control thrust control of linear induction motor," in *Proc. IEEE Ind. Appl. Conf.*, 2000, vol. 3, pp. 1655–1661.

[14] M. Pucci, A. Sferlazza, G. Vitale, and F. Alonge, "MRAS sensorless techniques for high performance linear induction motor drives," presented at the IEEE Int. Power Electron. Motion Control Conf., Orhid, Macedonia, Sep. 6–8, 2010.

[15] M. Cirrincione, M. Pucci, A. Sferlazza, and G. Vitale, "Neural based MRAS sensorless techniques for high performance linear induction motor drives," in *Proc. 36th Annu. Conf. Ind. Electron. Soc.*, Nov. 7–10, Phoenix, AZ, pp. 918–926.

[16] C. Shauder, "Adaptive speed identification for vector control of induction motors without rotational transducers," *IEEE Trans. Ind. Appl.*, vol. 28, no. 5, pp. 1054–1061, Sep./Oct. 1992.

[17] M. Cirrincione, M. Pucci, G. Cirrincione, and G. A. Capolino, "A new TLS based MRAS speed estimation with adaptive integration for high performance induction motor drives," *IEEE Trans. Ind. Appl.*, vol. 40, no. 4, pp. 1116–1137, Jul./Aug. 2004.

[18] M. Cirrincione, M. Pucci, G. Cirrincione, and G. Capolino, "Sensorless control of induction machines by a new neural algorithm: The TLS EXIN neuron," *IEEE Trans. Ind. Electron.*, vol. 54, no. 1, pp. 127–149, Feb. 2007.

[19] J. Duncan,, "Linear induction motor-equivalent- circuit model," *IEE Proc.-Electr. Power Appl.*, vol. 130, no. 1, pp. 51–57, 1983.

[20] G. Cirrincione, M. Cirrincione, J. Hérault, and S. Van Huffel, "The MCA EXIN neuron for the minor component analysis: Fundamentals and comparisons," *IEEE Trans. Neural Netw.*, vol. 13, no. 1, pp. 160–187, Jan. 2002.

[21] G. Cirrincione and M. Cirrincione, *Neural-Based Orthogonal Data Fitting: The EXIN Neural Networks*. New York: Wiley, 2010.

[22] R. M. Pai, I. Boldea, and S. A. Nasar, "A complete equivalent circuit of a linear induction motor with sheet secondary," *IEEE Trans. Magn.*, vol. MAG-24, no. 1, pp. 639–654, Jan. 1988.

[23] E. F. da Silva, E. Bueno dos Santos, P. C. M. Machado, and M. A. A. de Oliveira, "Dynamic model for linear induction motors," in *Proc. IEEE Int. Conf. Ind. Technol.*, Maribor, Slovenia, Dec.2003, pp. 478–482.

[24] J. H. Sung and K. Nam, "A new approach to vector control for a linear induction motor considering end effects," in *Proc. IEEE 34th IAS Annu. Meet. Ind. Appl. Conf.*, 1999, vol. 4, pp. 2284–2289.

[25] G. Kang and K. Nam, "Field-oriented control scheme for linear induction motor with the end effect," *IEE Proc.-Electr. Power Appl.*, vol. 152, no. 6, pp. 1565–1572, Nov. 2005.

[26] V. Isastia, G. Gentile, S. Meo, A. Ometto, N. Rotondale, and M. Scarano, "A voltage feeding algorithm for vectorial control of linear asynchronous machines taking into account end effect," in *Proc. Int. Conf. Power Electron. Drives Energy Syst. Ind. Growth*, 1998, vol. 2, pp. 729–734.

[27] I. Takahashi and Y. Ide, "Decoupling control of thrust and attractive force of a LIM using a space vector control inverter," *IEEE Trans. Ind. Appl.*, vol. 29, no. 1, pp. 161–167, Jan./Feb. 1993.

[28] M. Cirrincione, M. Pucci, G. Cirrincione, and G. A. Capolino, "A new adaptive integration methodology for estimating flux in induction machine drives," *IEEE Trans. Power Electron.*, vol. 19, no. 1, pp. 25–34, Jan. 2004.

[29] J. Holtz and Q. Juntao, "Sensorless vector control of induction motors at very low speed using a nonlinear inverter model and parameter identification," *IEEE Trans. Ind. Appl.*, vol. 38, no. 4, pp. 1087–1095, Jul./Aug. 2002.

[30] J. Holtz and Q. Juntao, "Drift- and parameter-compensated flux estimator for persistent zero-stator-frequency operation of sensorless-controlled induction motors," *IEEE Trans. Ind. Appl.*, vol. 39, no. 4, pp. 1052–1060, Jul./Aug. 2003.

[31] M. Comanescu and L. Xu, "Sliding-mode MRAS speed estimators for sensorless vector control of induction machine," *IEEE Trans. Ind. Electron.*, vol. 53, no. 1, pp. 146–153, Feb. 2006.

[32] G. Gentile, N. Rotondale, and M. Scarano, "Analisi del funzionamento transitorio del motore lineare," *L'Energia Elettrica*, no. 5, Nov. 1987.

[33] G. Gentile, N. Rotondale, and M. Scarano, "The linear induction motor in transient operation," *L'Energia Elettrica*, nos. 7–8, 1988.

Maurizio Cirrincione (M'03–SM'10) received the Laurea degree in electrical engineering from the Politecnico of Turin, Turin, Italy, in 1991, and the Ph.D. degree in electrical engineering from the University of Palermo, Palermo, Italy, in 1996.

In 1996, he was a Researcher at the Institute on Intelligent Systems for the Automation, Italian National Research Council, Palermo. Since September 2005, he has been a Professor at the University of Belfort Mobeliard, Belfort, France. His current research interests include neural networks for modeling and control, system identification, intelligent control, electrical machines, and drives.

Dr. Cirrincione received the "E.R.Caianiello" prize for the best Italian Ph.D. thesis on neural networks in 1996.

Angelo Accetta (M'08) received the Laurea degree in electrical engineering from the University of Palermo, Palermo, Italy, in 2008, where since 2008, he has been working toward the Ph.D. degree in the Department of Electrical Engineering, Electronics and Telecommunications.

He is also with the Institute on Intelligent Systems for the Automation, Italian National Research Council, Palermo, Italy. His current research interests include electrical machines, control techniques of electrical drives, intelligent control, power converters, and fuel cell system control and diagnosis.

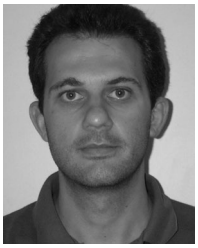

Marcello Pucci (M'03–SM'11) received the Laurea and Ph.D. degrees in electrical engineering from the University of Palermo, Palermo, Italy, in 1997 and 2002, respectively

In 2000, he was a host student at the Institut of Automatic Control, Technical University of Braunschweig, Braunschweig, Germany, where he was involved in the field of control of ac machines, with a grant from Deutscher Akademischer Austauscdienst—German Academic Exchange Service. From 2001 to 2007, he was a Researcher at the Institute on Intelligent Systems for the Automation, Italian National Research Council, Palermo, where since 2008, he has been a Senior Researcher. His current research interests include electrical machines, control, diagnosis and identification techniques of electrical drives, intelligent control, and power converters.

Dr. Pucci serves as an Associate Editor of the IEEE TRANSACTIONS ON INDUSTRIAL ELECTRONICS and the IEEE TRANSACTIONS ON INDUSTRY APPLICATIONS. He is a member of the Editorial Board of the *Journal of Electrical Systems*.

Gianpaolo Vitale (M'04) received the Laurea degree in electronic engineering from the University of Palermo, Palermo, Italy, in 1988.

From 1994 to 2001, he was a Researcher at the Institute on Intelligent Systems for the Automation, Italian National Research Council, Palermo, where since 2002, he has been a Senior Researcher. From 1999 to 2007, he was a Professor of power electronics and applied electronics at the Engineering Faculty of Palermo. He was the Supervisor of a research project on electromagnetic compatibility of electric drives and of a research project on intelligent management of electric energy supplied by renewable sources. His current research interests include the fields of power electronics and related problems of electromagnetic compatibility.

Mr. Vitale is a Member of the IEEE Vehicular Technology Society, the IEEE Industrial Electronics Society, and the IEEE Electromagnetic Compatibility Society. He serves as a Reviewer for several journals and conferences.